



HHS Public Access

Author manuscript

Biomaterials. Author manuscript; available in PMC 2016 June 01.

Published in final edited form as:

Biomaterials. 2015 June ; 52: 395–406. doi:10.1016/j.biomaterials.2015.02.034.

Actin Grips: Circular Actin-Rich Cytoskeletal Structures that Mediate the Wrapping of Polymeric Microfibers by Endothelial Cells

Desiree Jones^a, DoYoung Park^b, Mirela Anghelina^a, Thierry Pecot^{a,b,+}, Raghu Machiraju^b, Ruipeng Xue^c, John Lannutti^c, Jessica Thomas^d, Sara Cole^e, Leni Moldovan^a, and Nicanor I. Moldovan^{a,*}

^aDepartment of Internal Medicine, The Ohio State University, Columbus, OH, 43210, USA

^bDepartment of Computer Sciences and Engineering, The Ohio State University, Columbus, OH, 43210, USA

^cDepartment of Materials Sciences, The Ohio State University, Columbus, OH, 43210, USA

^dDepartment of Biomedical Engineering, The Ohio State University, Columbus, OH, 43210, USA

^eDepartment of Campus Microscopy and Imaging Facility, The Ohio State University, Columbus, OH, 43210, USA

Abstract

Interaction of endothelial-lineage cells with three-dimensional substrates was much less studied than that with flat culture surfaces. We investigated the *in vitro* attachment of both mature endothelial cells (ECs) and of less differentiated EC colony-forming cells to poly-ε-capro-lactone (PCL) fibers with diameters in 5–20 μm range ('scaffold microfibers', SMFs). We found that notwithstanding the poor intrinsic adhesiveness to PCL, both cell types completely wrapped the SMFs after long-term cultivation, thus attaining a cylindrical morphology. In this system, both EC types grew vigorously for more than a week and became increasingly more differentiated, as shown by multiplexed gene expression. Three-dimensional reconstructions from multiphoton confocal microscopy images using custom software showed that the filamentous (F) actin bundles took a conspicuous ring-like organization around the SMFs. Unlike the classical F-actin-containing stress fibers, these rings were not associated with either focal adhesions or intermediate filaments. We also demonstrated that plasma membrane boundaries adjacent to these circular cytoskeletal structures were tightly yet dynamically apposed to the SMFs, for which reason we

© 2015 Published by Elsevier Ltd.

This manuscript version is made available under the CC BY-NC-ND 4.0 license.

*Corresponding Author: Nicanor I. Moldovan, Ph.D., Department of Internal Medicine, Division of Cardiovascular Medicine, 460 W. 12 Ave, Room 306, Biomedical Research Tower, Ohio State University, Columbus, OH 43210, tel. 614-247-7801, fax 614-247-7799, nmoldova@yahoo.com.

⁺Current Address: Institut des Sciences Chimiques de Rennes - UMR6226, Campus de Beaulieu, 263 Avenue Général Leclerc, 35042 Rennes, France

Publisher's Disclaimer: This is a PDF file of an unedited manuscript that has been accepted for publication. As a service to our customers we are providing this early version of the manuscript. The manuscript will undergo copyediting, typesetting, and review of the resulting proof before it is published in its final citable form. Please note that during the production process errors may be discovered which could affect the content, and all legal disclaimers that apply to the journal pertain.

suggest to call them ‘actin grips’. In conclusion, we describe a particular form of F-actin assembly with relevance for cytoskeletal organization in response to biomaterials, for endothelial-specific cell behavior *in vitro* and *in vivo*, and for tissue engineering.

Introduction

Hybrid constructs containing cells and fibrillar scaffolds are increasingly used as models of cellular interaction with extracellular matrix [1], or for various bioengineering applications [2, 3]. Because of their favorable biomimetic and biomechanical properties, cell-seeded fibrillar scaffolds are considered for vascular grafting [4], as cardiovascular patches [5, 6], or for bone reconstruction [7]. Constructs containing endothelial cells (ECs) are of particular interest, due to their relevance for vascular development and repair [6]. However, the fibrillar substrates generally used for ECs retention have diameters within either the nanometer size range [8], or larger than 50 μm [9]. This leaves a gap in our understanding of the interaction of ECs with fibers having diameters within the cell-size range (5–20 μm). Wrapping of ‘objects’ that have diameters comparable to the cells’ diameter, such as other capillaries, was proposed as a mechanism for microvascular anastomosis *in vivo* [10], but an *in vitro* model suitable for studying this process has yet to be developed. Moreover, there is a growing interest in how cell morphology and/or biomechanics concur with transcriptional and signaling pathways in regulating cellular functions such as survival, proliferation, differentiation, migration, response to stimuli, and tissue organization [11]. Thus, the attachment of cells to fibrillar scaffolds could be a method to impose shape and/or tension constraints on cells. Using it, we previously demonstrated that mesenchymal stem cells aligned by a micro-fibrillar substrate have an increased expression of cardiac differentiation-specific genes [5].

Recently we [12] and others [13] have also found that ECs incubated with polymeric scaffold microfibers (SMFs) within their own size range re-organize their actin cytoskeleton in bands oriented transversally to cylinder’s axis. In the current study, we further address the mechanisms facilitating this interaction, specifically the occurrence and maintenance of a tubular morphology in this cellular system, by focusing on the organization of F-actin as a dynamic cytoskeletal component. At the scale of interest here, ECs are organized *in vivo* as tube-shaped components of capillaries or small arterioles [14]. *In vitro*, ECs can also be induced to adopt a substrate-dependent curvature. This was shown to determine the organization of extracellular matrix secreted by endothelial-lineage cells attached to fibers with diameters in the tens/hundreds of micrometers range in a transversal, banded pattern, independent of the orientation of the cytoskeleton (actin remaining aligned longitudinally) [9]. A transversal distribution of extracellular matrix was also found in human umbilical vein ECs (HUVECs), but not in the more primitive endothelial colony forming cells (ECSFs), attached to electrospun poly- ϵ -caprolactone (PCL) scaffolds with fibers below 10 μm in diameter [13].

Moreover, it was reported that human brain microvascular ECs seeded on collagen-coated glass rods with diameters close to 10 μm , completely wrap around their support, unlike HUVECs [15], or human fibroblasts in similar settings [16]. This behavior made the authors

assume that high-curvature substrate wrapping is a unique property of the brain capillaries [15]. This claim conflicts with other reports on HUVECs behavior, showing that these cells could fully reel around collagen struts within the same range of dimensions, and consequently modify the orientation of their actin filaments [17].

Although ultimately being a property of the F-actin bundles themselves (as shown by an elegant biomechanical model [18]), the impact of support's curvature on the cytoskeleton-dependent cell morphology is likely to be further compounded by a material's adhesiveness for cells. For example, PCL used in tissue engineering applications for its multiple material qualities, has poor cellular adhesiveness [19–23]. In fact, the PCL films required a chemical modification by macromolecular covalent modification [19, 20] or alkalization [21, 22], to become an optimal culture support comparable with tissue culture polystyrene (TCPS) for HUVECs [19–21] and for human ECFCs [22], respectively. However, the behavior of EC-lineage cells on PCL scaffolds only recently started to be explored [12, 13].

Our analysis of ECs and of ECFCs engaged with SMFs prepared from non-modified PCL helps explain how these cells adapt to a geometrically unusual environment, also shedding light on their behavior in analogous situations *in vivo*. The answer resides in the profound reorganization of the actin cytoskeleton, which could biomechanically compensate for the reduced biochemical adhesiveness.

Materials and Methods

2.1 Scaffold preparation

Scaffolds with fibers 1–10 μm in diameter were prepared by electrospinning as previously described [24]. In brief, 8–11 % (by weight) PCL solutions were prepared by dissolution in 35°C dichloromethane via continuous stirring. After cooling to room temperature, the solution was placed in a 60-cc syringe with a 20-gauge blunt tip needle and electrospun using a high voltage DC power supply set to 23 kV, a 20 cm tip-to-substrate distance and a 15 mL/h flow rate. Electrospinning was conducted in a chamber in which the relative humidity was maintained above 90%. The electrospun fibers were deposited onto aluminum foil for 15 min; the fiber sheet was then placed in a vacuum overnight to ensure the removal of residual solvent. 18 mm \times 18 mm samples were cut and glued at the edges on glass coverslips for imaging analysis.

2.2 Cells and incubations with scaffolds

HUVECs were purchased from ScienCell (Carlsbad, CA) and cultured in ECM (ScienCell). ECFCs were purchased from Lonza (Allendale, NJ) and cultured in EGM-2 (Lonza). Cells were grown in tissue culture polystyrene T-75 flasks until they reached 80% confluence, when they were trypsinized and seeded on coverslips and PCL scaffolds for time intervals ranging from 24 h to 10 days. During this time, the cells were incubated at 37°C and the medium was changed bi-weekly.

2.3 Endothelial differentiation assay

RNA was extracted from HUVEC grown in ECM either on TCPS, or on PCL scaffolds for 1–7 days, using RNeasy Mini Kit (Qiagen, Valencia, CA) according to the manufacturer's protocol, tested for quality, and stored at -80°C until use. Primers (SABiosciences/Qiagen) were diluted 1:20 with molecular-grade water, and $5\ \mu\text{L}$ /well were added to 384-well plates using a Biomek[®] FX Laboratory Automation Workstation (Beckman Coulter, Inc., Brea, CA). The plates were left to dry overnight in a sterile hood and stored covered at -20°C until use. Quantitative real-time PCR (qRT-PCR) was performed using SYBR Green (SABiosciences/Qiagen) and a 7900HT Real-Time PCR System (Applied Biosystems/Life Technologies, Foster City, CA) operated in standard mode. All of the PCR runs contained a dissociation step. The samples were amplified in duplicate in a total volume of $5\ \mu\text{L}$. The results are expressed as the relative copy number (RCN), defined as $\text{RCN} = 2^{-\text{Cq}} \times 100$, where Cq is the difference $\text{Cq}(\text{target}) - \text{Cq}(\text{reference})$ [25]. As a reference for normalization, we used the median Cq values of four endogenous controls. We analyzed the expression of a set of the following 21 genes comprising: (i) primitive markers (ABCG2, CD117/cKit, CD133/prominin, CD34, GATA4, NKX2-5, POU5F1/Oct4); (ii) vascular function-related markers (CD31/PECAM1, CAV3/caveolin3, CDH5/VE-cadherin, CNN1/calponin, FSHR/follicle stimulating hormone receptor, KDR/VEGFR2, NES/nestin [26], NOS3/eNOS, TEK/Tie2, VWF/von Willebrand Factor, as well as ACTA2/alpha actin, ALPL/alkaline phosphatase, COL1A1/collagen I); (iii) the proliferation-associated marker MKI67; and (iv) housekeeping genes B2M/beta-2 microglobulin, CAP1, GAPDH and RPL13 (as endogenous controls). For analysis, the genes were grouped in two clusters: ten with endothelial cell-relevant functions (Cluster 1), as objectively defined by gene expression covariation in our recent study [27] (CD31, CAV3, CDH5, CNN1, FSHR, KDR, NES, NOS3, TEK, VWF), and the remaining as endothelial-irrelevant genes (Cluster 2). The data for each gene at each time point were normalized to the corresponding values of the RCN obtained in two-dimensional cultures (time = 0), then averaged to generate separate indices, and displayed as dependent on time in culture, along with the MKI67 proliferation-associated gene.

2.4 Fluorescent staining

At the indicated time points, cells were fixed with 3.7% paraformaldehyde (PFA) and permeabilized with 0.1% Triton X-100 prior to immunocytochemistry. Anti-vinculin and anti-paxillin antibodies (Sigma-Aldrich, St. Louis, MO) were added and incubated at 4°C overnight. The following day, appropriate secondary antibodies (AlexaFluor 647-labeled, phalloidin-AlexaFluor 488, and DAPI - all from Life Technologies/Invitrogen, Grand Island, NY) were added. Actin was also visualized in TCPS- and scaffold-attached cells after transfection with a BacMam actin-GFP transduction reagent (Life Technologies/Invitrogen), according to the manufacturer's instructions.

Additionally, coverslip-attached scaffolds containing live cells were incubated with PKH26 (Sigma-Aldrich), a hydrophobic red fluorescent label [28]. The scaffolds were mounted in Fluoromount[™] (Sigma-Aldrich) and imaged using Olympus Filter FV1000 and Olympus Spectral FV1000 confocal systems (Olympus America Inc., Melville, NY). Images were viewed using the Olympus FV10-ASW software.

2.5 Phagocytosis assays

Trypsinized HUVEC were incubated in suspension, under plate rotation for 30 min at 37°C and 5% CO₂, with 3.5 µm diameter magnetic beads conjugated with a biotinylated mouse anti-human VEGF Receptor 2 (from MACSiBeads, Miltenyi, Auburn, CA), at a ratio of beads to cells of 20:1. The cells were then fixed, permeabilized as described, stained with AlexaFluor 488-Phalloidin and further incubated with an anti-mouse-AlexaFluor 543 antibody for detection of the beads, and with 2-(4-Amidinophenyl)-6-indolecarbamide dihydrochloride, 4',6-Diamidino-2-phenylindole dihydrochloride (DAPI, Sigma-Aldrich, St. Louis, MO) for visualization of nuclei.

Scaffolds containing live cells were also incubated with PKH26 (Sigma-Aldrich, St. Louis, MO), a hydrophobic red fluorescent label [28], dissolved either in the solution provided by the manufacturer to label the SFMs, or in phosphate buffer saline (PBS, pH 7.4), to induce its precipitation and to be phagocytosed by the cells.

2.6 Confocal laser scanning, multiphoton, and live cell time-lapse microscopy

Confocal laser scanning microscopy (CLSM) images of cell-seeded scaffolds were taken using the Olympus Spectral FV1000 confocal systems. The 488 nm krypton-argon laser was used for excitation of EGFP. Projected views of the confocal images were produced using Olympus FlowView v3.2 software. For live-cell imaging, transfected cells were seeded on 10% PCL scaffolds. Live cell imaging was performed using an Infinity3 2D array confocal scanner (Visitech Intl. Ltd.) equipped with an Olympus IX81 inverted microscope system and a 40× objective lens (N.A. 0.95). Normal cell culture medium was used during imaging. The cells were maintained at 37°C and 5% CO₂ throughout the process. Z stack images were acquired every 5 min for 1 hour. Image z-stacks were captured using a Hamamatsu C9100 EMCCD camera using MetaMorph software (Vers.7.6.0, Molecular Devices, Sunnyvale, CA).

2.7 Image analysis

Digital unwrapping of the F-actin bundles from the SMFs was performed using either a Matlab program that projects the space around a cylinder on a plane [15] or, to section this space with planes parallel to cylinders' axis, our original method [12]. In addition, to determine the properties of the scaffold inductive of cell attachment, we compared fiber diameters at cell-attachment site with overall distribution of fiber diameters in the scaffold. In brief, segmented 3D images of cell-seeded scaffolds stained with PKH26, extracted from digitized confocal images, were fitted with 1-µm long template cylinders of pre-determined diameters, as described in detail in our method paper [12]. Normalized histograms of these distributions were compared for dissimilarity by the Q-Q plot method [29]. Nuclear roundness was measured by applying Principal Component (PC) Analysis [30] to the points composing the nuclei, as the ratio of the largest PC vs. the 3rd largest PC (a value of 1 corresponds to round cells). The nuclei were identified in digitized DAPI-stained three-dimensional confocal images by our original non-parametric segmentation algorithm [31].

***In vivo* implanted PCL scaffolds and Matrigel plugs**—PCL scaffolds and Matrigel plugs were implanted subcutaneously in C57-B16 mice as previously described [32], and

retrieved after six weeks. To maintain the native cellular architecture and to image the interaction in three dimensions, minimally dissected, non-sectioned preparations were fixed immediately and stained in situ by immersion with phalloidin-Alexa 488 and counter-stained with DAPI, as described. Whole specimen fragments were mounted under optical coverslips and depth-imaged with an Olympus FV1000 Mutiphoton microscope equipped with a 25× objective lens (N.A 1.05). The images were processed with the Olympus FV10-ASW software.

2. 8 Data analysis

Statistics (t-Test) were performed using the Microsoft Excel 2010 capabilities. Data were presented as means \pm SD and a $p < 0.05$ was considered significant.

Results

3.1 F-actin organization within endothelial cells attached to PCL scaffolds

Two-dimensional PCL films are well known as poorly adhesive substrates for cell cultivation, including endothelial and smooth muscle cells [19–22]. However, HUVECs could easily attach to SMFs prepared from PCL by electrospinning in micro-fibrillar form [12, 13]. Using scanning electron microscopy (SEM), we identified cells attached directly to individual SMFs, or more seldom simultaneously to multiple fibers of smaller diameters (Fig. S1). Notably, on single SMFs, the cells displayed a very attenuated morphology, including that of nuclei, barely detectable in relief (Fig. S1). HUVECs grew vigorously on SMFs for at least 10 days, covering all available space (Fig. S2A), even when they were incubated without any pre-treatment of the scaffold, or without addition of soluble adhesiveness-enhancing factors, besides those present in the culture medium.

When grown on polystyrene tissue plates as slightly subconfluent culture, HUVECs developed the commonly linear stress fibers, as well as marginal actin-rich ruffles (Fig. 1A). However, as we [12] and others [13] have previously reported, in the cells that intimately engage individual SMFs F-actin is distributed not solely as classical stress fibers (i.e. longitudinally aligned with the scaffold's fiber length), but also as transversal bands (Fig. 1B,C). This pattern of microfilament organization was present in various degrees (Fig. S2B), in a proportion that increased with time in culture, both in HUVECs and - in our hands, unlike in [13] - in the more primitive ECFCs (Fig. 1D), although at similar times in culture less frequently in the latter.

To understand how SMF diameter influences cell attachment, we extracted the distribution of SMFs diameters and that of the associated nuclear shape directly from 3D confocal images, specifically at HUVECs attachment sites (Fig. 2), using an original software described in [12] and [31], respectively. Counterintuitively, we found that HUVECs did not grow preferably on larger-diameter branches of the scaffold (Fig. 2A). Moreover, this analysis showed that the nuclear shape also depended on SMF diameters, becoming slightly rounder as this diameter increased (Fig. 2B). Considering that the nuclear shape follows that of the whole cell [33] as effect of a direct interaction of nuclei with F-actin filaments [34], these observations combined imply that the thinner SMFs are conducive to flatter cells, i.e.

that fiber's curvature indeed controls EC-substrate interaction as suggested [15, 18], for reasons explored below detailed below.

3.2 Circularity of F-actin distribution within scaffold-wrapping ECs

We further analyzed the three-dimensional distribution of F-actin microfilaments in scaffold-wrapping cells, to determine the extent of circumferential coverage of the SMFs with ECs, a property never quantified before. In cells incubated for longer time (10 days) with SMFs, we documented by digital unwrapping of confocal images a fully circumferential continuity of the majority of F-actin bands (Fig. 3A). This pattern corresponded to three-dimensional rings that occasionally crossed the nuclei (Fig. 3Ac). We could also find within the scaffold-wrapping ECs at earlier stages of cell attachment (1–2 days in culture) pools of loosely but circularly organized F-actin filaments (Fig. 3Ba,b), by digitally sectioning with cylindrical planes the space around SMFs, followed by their 2D projection ('layered unwrapping') (Fig. 3c,d).

In certain instances however, even in long-term cultures we could see interlaced fragments of F-actin filaments in 3-to-2 dimensional projections (Fig. 3Ac), or in optical sections (Fig. 4, arrowheads). Often these filament bundles were oriented obliquely with respect to the long axis of the SMF, and did not fully surround the cylinder, for which reason we previously named them 'concave actin bundles' (CAVs) [12]. The cytoplasm itself of these cells still fully wrapped the supporting SMF, as inferred from the co-existence in the same cell of complete F-actin rings (Fig. 3Ac and 4, arrows). We assume these oblique CAVs represent stages in rings' assembly, a process which may start with longitudinally oriented stress fibers, that progressively bend and at the same time reorient in a transversal position, as proposed by a theoretic biomechanical model [18].

3.3 Role of F-actin rings in 'gripping' the micro-fibrillar support

Direct confocal optical sectioning also revealed that HUVECs engaged with the scaffold for long intervals displayed their transversally-banded F-actin more often and/or more intense at the cell's extremities (Fig. 5A). The non-marginal (internal) microfilaments were generally thinner F-actin structures, which sometimes had a heavily beaded aspect, occasionally with the conspicuous oblique pattern (e.g. Fig. 5A, C). In isolated cells, F-actin located at cell's ends occasionally appeared undulated (Fig. 5B), reminiscent of lamellipodial actin ruffles that we described at the leading edges of migrating ECs [35]. Therefore intriguingly, the cells' attachment to SMFs could still be compatible with some form of cell motility along the fibers in a sleeve-sliding mode, at least in sparse-seeding conditions.

Ring-containing fiber-wrapping cells usually displayed an elongated and attenuated morphology, including that of the nuclei (Fig. 5B), in concordance with the SEM images (Fig. S1). In line with the known biomechanical coupling between the cytoskeleton and nucleus [36], this could be the result of a pressure exerted over the nuclei by (or via the cytoplasm with the contribution of) these F-actin rings (Fig. 2Ac).

We further tested the hypothesis that the circularly-organized actin microfilaments could indeed play a role in stabilizing the attachment ECs to their cylindrical substrates. This possibility was suggested by several lines of evidence (expanded below), including their

presence in all partitions of the cytoplasm of single cells that separately wrapped different intersecting SMFs (Fig. 5C).

To estimate the tightness of cells' attachment to SMFs, we incubated in different experiments live HUVECs (pre-seeded on scaffolds for 10 days), with the hydrophobic fluorescent label PKH26. We found that PKH26 strongly labeled the SMFs in regions not occupied by cells (Fig. 5D–F), and very faintly - if at all (Fig. 5F) - the cellular plasma membranes [28]. Notably, the transition between stained and unstained portions on SMFs were very sharp, and always limited by nearby F-actin rings (Fig. 5D–F). This let us assume that the F-actin rings created an effective barrier for lateral diffusion of the dye in the space occupied by SMF-attached cells (compare Fig. 5E with 5F). The tight contact between the cells and fibers at the rings' level, which thus 'gripped' the scaffold, prevented the diffusion of the soluble dye underneath the cells. However, SMFs were not protected from the dye when the cells did not wrap the fiber and therefore did not form rings (Fig. 5E–F, arrowheads). To indicate their putative role in cell-fiber interaction, we suggest to name these SMF-induced cytoskeletal rings as 'actin grips' (AGs).

3.4. Relationship between AGs formation and cell's phagocytic activity

ECs belong, together with the professional macrophages, to the 'reticulo-endothelial system' [37], both cell types and other epithelial cells being capable of consistent phagocytosis [38]. Thus, we expected that HUVECs likewise engage in a phagocytic activity triggered by their substrate, when attached to SMFs. In principle this could explain the wrapping of SMFs by these cells as a failed attempt to engulf the PCL fibers, or a 'frustrated phagocytosis'. To study this mechanism, we first performed a direct test of phagocytosis, where beads of ~4 μm , a size comparable with the preferred fiber diameters at the attachment sites (Fig. 2A), covered with an anti-VEGF receptor 2 (a molecule abundantly present on ECs [39]) antibody, were incubated in suspension with HUVECs (Fig. S3A). We found that indeed these beads were taken up in F-actin limited, U-shaped phagocytic 'cups', and internalized into fully closed vesicles (Fig. S3B, C). However, the F-actin layer deployed around these *bona-fide* phagocytic particles had a very different texture, being much more uniform in thickness and in granularity, compared to AGs.

Next we studied the uptake by scaffold-attached HUVECs of a smaller particulate phagocytic marker, prepared from the same fluorescent label PKH26 (suspended in a more hydrophilic buffer, to induce its aggregation [28]), as routinely used as a phagocytosis assay. We found that in SMF-attached HUVECs the PKH26 particles accumulated within compartments laterally separated by AGs, without any detectable F-actin at the fiber-cell interface (Fig. S3D,E). If AGs formation represented a similar response of the cells to internalized objects, they should have been distributed as a uniform layer of F-actin continuously distributed along the SMFs, which was not the case.

We also reasoned that if the organization of F-actin in SMF-attached cells was simply the result of a frustrated phagocytosis, then AGs should readily appear during SMFs interaction with professional phagocytes and/or ECs *in vivo*, a situation occurring during 'foreign body reaction' [40]. In reality, AGs were completely absent in the macrophages and macrophage-derived giant cells attached to PCL scaffolds that we retrieved from mice after subcutaneous

implantation (Fig. S4A). Conversely, in neovascularization-inducing hydrogel (Matrigel) plugs subcutaneously implanted in mice [32], we did find in the developing capillary ECs, although very seldom, F-actin bands with a transversal distribution, in a pattern reminiscent of, but different from, that of AGs (Fig. S4B).

3.5 Relationship of AGs with focal adhesions and intermediate filaments

Since the stress fibers are routinely associated with focal adhesions (FAs) at their plasma membrane attachment site to substrate [41], we analyzed in SMFs-attached cells the presence and localization of the FA components paxillin and vinculin. While these proteins were both readily detectable at the ends of stress fibers in cells adherent to a flat tissue culture surface (e.g. Fig. S5A for paxillin), as well as at the extremities of actin microfilaments distributed longitudinally on scaffolds, both of these FA molecules were absent in well-developed, fully assembled AGs (Fig. 6A–D). Absence of AG-associated FAs was consistent with the morphological observation that the circular F-actin bundles could be organized as relatively thick, continuous bands placed within the cytoplasm at a distance from the plasma membrane in contact with the SMF (Fig. 3B).

Furthermore, in flat-surface attached cells the stress fibers are often reinforced by co-localization with intermediate filaments [42] (e.g. vimentin-containing intermediate filaments, Fig. S5B). However, in the scaffold-attached HUVECs, vimentin-positive intermediate filaments were absent from the cytoplasm regions occupied by AGs (Fig. 6E,F). At the same time alpha-actinin, a standard component of contractile F-actin microfilaments [43], was readily detectable in AGs by immunocytochemistry (Fig. 6G).

Fig. 6G also illustrates a key finding of this study, that AGs occurred only (although not always) in cells attached to fibers with a diameter comparable to cells' size, implying cylindrical wrapping. HUVEC engaging fibers with larger diameters had most of their F-actin organized in stress fibers and/or peripheral bundles (Fig. 6G), in a fashion similar to those attached *in vitro* to a flat surface (e.g., Fig. 1A), or as part of the intima of larger diameter blood vessels *in vivo*. Thus, substrate's curvature is a necessary condition [18], but not sufficient to explain the formation of AGs, which in addition seem to require a full fiber wrapping that generates a cylindrical cell shape.

3.6 Dynamics of F-actin-containing structures in SMFs-attached cells

In fully differentiated ECs that intimately wrap the SMFs in culture, AGs represented the majority of F-actin (Fig. S2A). However, AGs may co-exist with longitudinally-oriented F-actin in same cells, in adjacent cells located on the same fibers, or on fibers of similar diameter (Fig. S2B). This suggests that either the mechanisms of AGs formation is more complex than a simple reaction to curvature as proposed [15, 18], or that it indicates a slow progressive reorganization of F-actin from one assembly form into another. A dynamic AGs formation and disassembly would be also compatible with a migratory polarization of SMF-wrapping cells, as suggested by Fig. 5B.

For this reason, we directly investigated the dynamics of the F-actin based cytoskeletal structures in live cells. To this end, we transfected HUVECs attached to culture dishes with

a GFP-actin expressing vector, and then transferred them on PCL scaffolds. As expected, in 2-dimensional cultures GFP-labeled actin monomers became incorporated into *bona-fide* stress fibers and in marginal ruffles (Fig. S5C). We then imaged live individual AG-containing cells by time-lapse fluorescence microscopy. We focused on an AG located centrally within a scaffold-attached cell, which slowly disintegrated over a one-hour time span, while other actin-dense structures simultaneously developed at cell margins (Fig. 7A). Because the cell was placed at the intersection of three fibers, the system was mechanically unstable, thus permitting observation of the consequences of an AG's dissolution. We analyzed time-dependently the pixel intensity in selected regions of the cell (Fig. 7B), an approach that confirmed that the F-actin patch seen in optical cross-section in the central upper side of the SMF, as well as the one underneath it, belonged to the same AG (as the GFP-actin fluorescence intensity decreased perfectly in parallel). Coincidentally, F-actin intensity followed a different, although temporally coordinated kinetics in other parts of the cell (encircled, Fig. 7B). Simultaneously, the cell's length became progressively reduced on the main attachment fiber, while extending on the perpendicular direction (Fig. 7C). These geometrical changes were in accordance with a model of SMFs constriction by AGs, and of loss of gripping power coincident with their disintegration, letting other tensions within the cell to be manifested.

3.7 Relationship between AGs formation and differentiation status of HUVECs

The observation that the frequency of AGs increased with time in culture, both in HUVECs and in ECFCs, raised the question whether this property was cell differentiation-dependent. AGs-induced cell flattening by itself, reflected in a corresponding nuclear deformation, was expected to impact on chromatin structure and thus on gene expression, thus modulating the differentiation status [34]. These considerations prompted us to analyze the time-dependent expression of endothelial-specific genes in HUVECs cultivated on scaffolds, as compared to those maintained in regular 2D culture. We found that the genes for a set of vascular function-related markers [27], that included VEGF receptor 2 (KDR), Tie-2, VE-cadherin (CDH5), eNOS (NOS3), von Willebrand factor, nestin, CD34, CD31(PECAM), c-Kit as well as alpha actin, were collectively expressed in the scaffold-wrapping cells at levels comparable to or higher than those in cells on flat surfaces (Fig. 8). At the same time, the transcriptional activity of a panel of endothelium-irrelevant genes (see ref. [27] and Methods), along with that of the proliferation marker MKI67 were reduced (Fig. 8). Combined, this multiplexed transcriptional profiling was indicative of a comparable or even more differentiated endothelial phenotype during SMFs cultivation, than in comparably subconfluent cells, maintained in two-dimensional cultures.

Discussion

The main finding of this study is that ECs have a phenotype-specific ability to fully wrap supports with diameters comparable to those of capillaries, even when the adhesiveness is intrinsically poor, such as for PCL. This cylindrical morphology was accompanied by the progressive reorganization of the actin-rich filaments in a ring pattern. For their putative role in cell interaction with SMFs and/or stabilization of their tubular shape, we named these

structures ‘actin grips’ (AGs; the simpler term ‘actin rings’ is already in use to define the peripheral actin bands present in epithelial cells [44], or in the cytokinetic furrows [45]).

To our knowledge, although a distribution of F-actin transversal to the cell’s cylindrical support has been reported before, the whole fiber-wrapping behavior involving just one cell, was not observed in other cell types besides ECs [15, 17]. For example, when fibroblasts were seeded on cylinders with a small curvature, they oriented longitudinally to avoid a sharp bending [16]. An influence of substrate curvature on morphology and orientation and F-actin organization within ECs adherent to collagen-coated glass rods with diameters varying from 10 to 500 μm was recently reported [15]. In this study, human brain microvascular endothelial cells readily wrapped the thinnest rods, and oriented a fraction of their actin microfilaments across the cylindrical axis. However, in this report HUVECs were said to resist bending and/or to change their shape, following the substrate curvature similarly to fibroblasts. HUVECs on rods covered with collagen of all diameters tested in this study systematically took an elongated morphology, and aligned with their long axis *parallel* to that of the cylindrical support, along with that of the majority of their actin [15]. In contrast, as we [12] and others [13] have previously showed, HUVECs incubated with PCL scaffolds could organize their F-actin in transversal bands. This seemingly contradictory behavior of HUVECs in geometrically comparable conditions highlights the importance of direct molecular adhesive interaction between the cells and their environment. Our results indicate that when the adhesive forces are suboptimal, ECs could still mount an engagement with a cylindrical substrate, mostly relying on biomechanical cues, i.e. by stabilizing their natural bending propensity with secondary cytoskeletal reinforcements.

In the current study we demonstrated that HUVECs on PCL fibers with diameters in the 5–15 μm range not only organize their actin cytoskeleton in a conspicuous ring-like pattern with predilection for localization at cells edges, but also efficiently wrap their cylindrical supports, thus ensuring a firm holding of the substrate. It would be surprising if such a sophisticated biomechanical mechanism existed only in *in vitro*, and did not have an *in vivo* counterpart. This could happen for instance when ECs need to wrap around a cylindrical substrate, during wrapping-and-tapping anastomosis [10]. In this case, a too strong adhesiveness would be counterproductive, because the wrapping cell must quickly disengage to slide laterally on top of the other cell, to expose their common lumens for fusion [10]. A migration while attached to SMFs was actually supported by one of our observations (Fig. 4B), indicative of migratory polarization in a fully wrapped cell.

The possibility of dynamic engagement with a cylindrical support may be facilitated by the likely *inverse* polarization status of the attracted cells: in a capillary, each EC is polarized with the apical side facing the fluid-filled lumen, and the basal one oriented towards the external side of the empty cylinder, where it is attached to the extracellular matrix-rich basal lamina. Others [46] and we [47] have shown that the morphological integration of the newly-formed capillaries with the immediate environment involves the interaction with the inner surface of a pre-existent cylindrical ‘tunnel’, as well as the synthesis and deposition of new, cell-derived basal lamina material [48]. For this reason, the attachment of ECs onto, and wrapping around, a solid SMFs is inverse to the normal topological configuration. This

may explain a weaker attachment and/or faster detachment, consistent with the absence of harder to disassemble focal adhesions.

4.1 Identity of AGs compared to other F-actin rich structures

Due to their unusual characteristics, we compared AGs with other F-actin-containing cellular structures. First, mature AGs do not seem to be stress fibers in the traditional sense, even if they might derive from those by re-orientation. Stress fibers are conspicuous cytoskeletal structures in culture, but *in vivo* are detectable primarily in shear-stressed ECs [49], and in general in tensed cells [50]. Second, in our system, a role for AGs in direct (biochemical) adhesion of ECs to SMFs is unlikely, because we could not co-localize with the AGs two FA-specific molecules, paxillin and vinculin, which were readily detectable at the extremities of actin filaments oriented alongside the scaffold. Furthermore, time-lapse microscopy observations on live cells suggest that AGs are more dynamic structures than the classical stress fibers. They also indicate that the actin monomers from a given AG could be exchanged with other F-actin containing structures within the same cell, as part of a tightly-controlled actin homeostasis [51], leading to complex forces within cells to be exerted on the scaffold (in our case, a contraction along the SMF). Consequently, our findings suggested that AGs may contribute to the maintenance of an *elongated* endothelial morphology on the fibrillar support, even in the absence of a FA-mediated adhesion, and that their dissolution may lead to modifications of cell shape.

Combined with their curvature, this role of AGs in cell shape control presumes a close interaction with the plasma membrane, a property of *bent* septin-containing actin bundles [45]. However, at individual fiber level, stress fibers are in general *linear* structures organized by fascin, while circularity in F-actin fibers is controlled by septins, recently identified to play a key role in organization of epithelial monolayers [52], in the formation of axon's F-actin rich transversal 'stripes' [53], or of the actin rings at furrows during cytokinesis [45]. However, we did not find a relationship between AGs frequency with any nuclear feature involved in cell division, nor a preferential placement of AGs at mid-cell position, as would be required for a role in cytokinesis. Instead, AGs could be more similar to dorsal stress fibers [54], to the 'actin arcs' present in lamellipodia and/or ruffles of migrating cells [55], or to the short-lived 'circular dorsal ruffles' induced by stimulation with growth factors [56], or by exposure to biaxial mechanical stretch [57]. In general, actin ruffles can be described as waves of concentrated F-actin, initiated at the cell periphery (usually the leading edge) and progressing backwards toward the cell's upper surface as the cell body advances forward [35]. In our case, AGs were localized mostly in the median (sometimes apparently crossing the nucleus) and in the basal portion of the cell body, coincident with a flat cell morphology, also reflected in the flatness of nuclei.

4.2. Possible roles of AGs *in vitro*

AGs seem to represent a unique cytoskeletal organization specifically adapted to the wrapping interaction of endothelial-lineage cells with solid, elongated objects with diameters comparable with that of cell's own size. An implication of our findings is that fiber wrapping may largely supply or even replace cells' need for direct adherence, required for survival [58]. In fact, we very seldom observed characteristically fragmented nuclei in

these cultures (data not shown). Instead, we witnessed a robust cell proliferation and covering of the PCL fibers, expanding from the initial patches to large surfaces after two weeks in culture, while flat surfaces covered with a PCL film showed poor cell-supporting (both attachment and survival) properties. This is because FAs provide the cells with a necessary anchor for attachment, and activate a pro-survival signaling program, while in their absence the cells enter a form of apoptosis called ‘anoikis’ [58]. Similar to our observation, mesenchymal stem cells cultivated on a 3D fibrillar scaffold of much larger diameter (more than 50 μm) also showed an enhanced survival, mediated by self-secreted laminin, although no wrapping and/or F-actin rings were observed in that case [59].

Here we demonstrate that this microfilament-based cytoskeletal structure is endothelial differentiation-dependent, because it is better represented in HUVEC than in the more primitive, cord-blood derived ECFCs, and their formation in scaffold attached HUVEC parallels the expression of endothelial-specific genes in these cells. In support of the differentiation dependence of AGs formation, a previous report indicates that ECFCs were unable to re-orient their actin transversally to the fiber’s cylinder, probably because those cells were prepared in the laboratory [13]. Our ECSFs were commercial, and thus more advanced in endothelial differentiation after their *in vitro* cultivation.

Due to the natural variation in a vessel’s size, ECs have shapes ranging from almost flat to cylindrical. However, most of the work addressing the properties of ECs used 2D *in vitro* models. Physiological implications of a cylindrical morphology of ECs have mostly been considered in gel-embedded cellular models. Still, the actual presence in these models of a true endothelial differentiation, including the formation of a patent (empty) capillary lumen, was often overlooked. This is due in part to the difficulty to induce and maintain the tubular shape in a controlled manner. Thus, our scaffold-based method could provide a simple and efficient method of ECs shape manipulation.

4.3. *In vivo* relevance of AGs

Besides the cardiovascular system [60], a cylindrical cell shape plays a preeminent role in the behavior of other cell types, particularly during developmental morphogenesis [61, 62]. We have previously investigated the acquisition of a tubular shape by endothelial progenitor cells and/or monocyte-macrophages during cell colonization of cylindrical tunnels *in vivo* [47]. This process is instrumental during sprouting-independent, progenitor cell-driven neovascularization [63]. In these cases, the tunnel diameter is also commensurate with that of colonizing cells, because the tunnels are formed by the proteolytic activity of matrix-penetrating cells of comparable size [64].

Indications of AGs presence in ECs *in vivo* is scarce at this time. This might be due to that fact that AGs are specialized structures, needed only when ECs wrap another object. This situation is not commonly encountered in normal capillaries, where constriction produced by AGs could actually pose a risk for occlusion. If so, it would be of substantial translational interest to explore the possible pathological AGs formation in several capillary obstructive conditions, currently attributed to the constrictive activity of pericytes [65]. However, AGs formation could be critical during the physiological fusion of two capillaries during their anastomosis by the proposed ‘wrapping-and-tapping’ mechanism, where one EC was

suggested to wrap around, and then to slide long another capillary [10]. If so, a deficient anastomosis due to inability to engage strongly enough the target microvessels, or to maintain the wrapping (e.g. due to a reactive oxygen-species induced actin polymerization perturbation in ECs as we have previously shown [35, 66]), may occur in the pro-oxidant conditions such as diabetes [67], leading to the microvascular rarefaction and/or to the perfusion deficits characteristic of this disease [68].

Conclusions

Here we studied the ring-like organization of actin-rich cytoskeletal bundles in mature ECs, during their full wrapping of cylindrical objects with diameters comparable with that of capillaries. We called these cytoskeletal rings ‘actin grips’ (AGs), due to their role in stabilizing the tubular shape of the cells attached to a poorly adhesive fibrillar material. We found AGs to be dynamical structures, apparently compatible with cell sliding in this fully wrapped state around the scaffold. The finding is surprising because it demonstrates a case of abundant F-actin bundles organization in a circular fashion with a constrictive capacity as well, a function reserved in ECs only to cytokinesis furrows, and to the peri-vascular contractile cells (namely, pericytes). Besides their possible roles during specialized activities in capillaries *in vivo*, which remains to be explored, AGs may also have multiple applications in tissue engineering, such as for stabilization of ECs interaction with the scaffolds used as cell carriers, for immuno-isolation of fibrillar scaffolds in order to mitigate their foreign body reaction and post-implantation immune responses, or for controlling ECs differentiation via substrate-driven gene expression.

Supplementary Material

Refer to Web version on PubMed Central for supplementary material.

Acknowledgments

Microscopy was performed in the Campus Microscopy and Imaging Facility of the Ohio State University, and qRT-PCR was performed in Nucleic Acids Shared Resource, Comprehensive Cancer Center of the Ohio State University. SEM imaging was performed at the Department of Materials Sciences and Engineering, College of Engineering, Ohio State University. This work was supported by NIH Grants R01 HL-096524 and RC2 AG-036559 to NIM.

References

1. Fischer SN, Johnson JK, Baran CP, Newland CA, Marsh CB, Lannutti JJ. Organ-derived coatings on electrospun nanofibers as ex vivo microenvironments. *Biomaterials*. 2011; 32:538–546. [PubMed: 20875916]
2. Kurobe H, Maxfield MW, Breuer CK, Shinoka T. Concise review: tissue-engineered vascular grafts for cardiac surgery: past, present, and future. *Stem Cells Transl Med*. 2012; 1:566–571. [PubMed: 23197861]
3. Singh S, Wu BM, Dunn JC. Enhancing angiogenesis alleviates hypoxia and improves engraftment of enteric cells in polycaprolactone scaffolds. *J Tissue Eng Regen Med*. 2013; 7:925–933. [PubMed: 22511397]
4. Roh JD, Sawh-Martinez R, Brennan MP, Jay SM, Devine L, Rao DA, Yi T, Mirensky TL, Nalbandian A, Udelsman B, Hibino N, Shinoka T, Saltzman WM, Snyder E, Kyriakides TR, Poerber JS, Breuer CK. Tissue-engineered vascular grafts transform into mature blood vessels via an

- inflammation-mediated process of vascular remodeling. *Proc Natl Acad Sci U S A*. 2010; 107:4669–4674. [PubMed: 20207947]
5. Guan J, Wang F, Li Z, Chen J, Guo X, Liao J, Moldovan NI. The stimulation of the cardiac differentiation of mesenchymal stem cells in tissue constructs that mimic myocardium structure and biomechanics. *Biomaterials*. 2011; 32:5568–5580. [PubMed: 21570113]
 6. Singh S, Wu BM, Dunn JC. Accelerating vascularization in polycaprolactone scaffolds by endothelial progenitor cells. *Tissue Eng Part A*. 2011; 17:1819–1830. [PubMed: 21395445]
 7. Roldan JC, Detsch R, Schaefer S, Chang E, Kelantan M, Waiss W, Reichert TE, Gurtner GC, Deisinger U. Bone formation and degradation of a highly porous biphasic calcium phosphate ceramic in presence of BMP-7, VEGF and mesenchymal stem cells in an ectopic mouse model. *J Craniomaxillofac Surg*. 2010; 38:423–430. [PubMed: 20189819]
 8. Zhang X, Thomas V, Xu Y, Bellis SL, Vohra YK. An in vitro regenerated functional human endothelium on a nanofibrous electrospun scaffold. *Biomaterials*. 2010; 31:4376–4381. [PubMed: 20199808]
 9. Barreto-Ortiz SF, Zhang S, Davenport M, Fradkin J, Ginn B, Mao HQ, Gerecht S. A novel in vitro model for microvasculature reveals regulation of circumferential ECM organization by curvature. *PLoS One*. 2013; 8:e81061. [PubMed: 24278378]
 10. Cheng G, Liao S, Kit WH, Lacorre DA, di TE, Au P, Fukumura D, Jain RK, Munn LL. Engineered blood vessel networks connect to host vasculature via wrapping-and-tapping anastomosis. *Blood*. 2011; 118:4740–4749. [PubMed: 21835951]
 11. Dike LE, Chen CS, Mrksich M, Tien J, Whitesides GM, Ingber DE. Geometric control of switching between growth, apoptosis, and differentiation during angiogenesis using micropatterned substrates. *In Vitro Cell Dev Biol Anim*. 1999; 35:441–448. [PubMed: 10501083]
 12. Park, DY.; Jones, D.; Moldovan, NI.; Machiraju, R.; Pecot, T. Robust Detection and Visualization of Cytoskeletal Structures in Fibrillar Scaffolds from 3-Dimensional Confocal Images. *IEEE Symposium on Biological Data Visualization*; Atlanta, GA. 2013. p. 25-32.
 13. Fioretta ES, Simonet M, Smits AI, Baaijens FP, Bouten CV. Differential response of endothelial and endothelial colony forming cells on electrospun scaffolds with distinct microfiber diameters. *Biomacromolecules*. 2014; 15:821–829. [PubMed: 24502702]
 14. Simionescu M, Simionescu N, Palade GE. Morphometric data on the endothelium of blood capillaries. *J Cell Biol*. 1974; 60:128–152. [PubMed: 4129076]
 15. Ye M, Sanchez HM, Hultz M, Yang Z, Bogorad M, Wong AD, Searson PC. Brain microvascular endothelial cells resist elongation due to curvature and shear stress. *Sci Rep*. 2014; 4:4681. [PubMed: 24732421]
 16. Dunn GA, Heath JP. A new hypothesis of contact guidance in tissue cells. *Exp Cell Res*. 1976; 101:1–14. [PubMed: 182511]
 17. Indolfi L, Baker AB, Edelman ER. The role of scaffold microarchitecture in engineering endothelial cell immunomodulation. *Biomaterials*. 2012; 33:7019–7027. [PubMed: 22796162]
 18. Biton YY, Safran SA. The cellular response to curvature-induced stress. *Phys Biol*. 2009; 6:046010. [PubMed: 19843983]
 19. Zhu Y, Gao C, Liu X, Shen J. Surface modification of polycaprolactone membrane via aminolysis and biomacromolecule immobilization for promoting cytocompatibility of human endothelial cells. *Biomacromolecules*. 2002; 3:1312–1319. [PubMed: 12425670]
 20. Zhu Y, Gao C, Shen J. Surface modification of polycaprolactone with poly(methacrylic acid) and gelatin covalent immobilization for promoting its cytocompatibility. *Biomaterials*. 2002; 23:4889–4895. [PubMed: 12361630]
 21. Serrano MC, Portoles MT, Vallet-Regi M, Izquierdo I, Galletti L, Comas JV, Pagani R. Vascular endothelial and smooth muscle cell culture on NaOH-treated poly(epsilon-caprolactone) films: a preliminary study for vascular graft development. *Macromol Biosci*. 2005; 5:415–423. [PubMed: 15895476]
 22. Serrano MC, Pagani R, Ameer GA, Vallet-Regi M, Portoles MT. Endothelial cells derived from circulating progenitors as an effective source to functional endothelialization of NaOH-treated poly(epsilon-caprolactone) films. *J Biomed Mater Res A*. 2008; 87:964–971. [PubMed: 18257077]

23. Fu X, Sammons RL, Bertoti I, Jenkins MJ, Dong H. Active screen plasma surface modification of polycaprolactone to improve cell attachment. *J Biomed Mater Res B Appl Biomater*. 2011
24. Nam J, Huang Y, Agarwal S, Lannutti J. Improved cellular infiltration in electrospun fiber via engineered porosity. *Tissue Eng*. 2007; 13:2249–2257. [PubMed: 17536926]
25. Gavrilin MA, Bouakl IJ, Knatz NL, Duncan MD, Hall MW, Gunn JS, Wewers MD. Internalization and phagosome escape required for Francisella to induce human monocyte IL-1beta processing and release. *Proc Natl Acad Sci U S A*. 2006; 103:141–146. [PubMed: 16373510]
26. Mokry J, Ehrmann J, Karbanova J, Cizkova D, Soukup T, Suchanek J, Filip S, Kolar Z. Expression of intermediate filament nestin in blood vessels of neural and non-neural tissues. *Acta Medica (Hradec Kralove)*. 2008; 51:173–179. [PubMed: 19271685]
27. Moldovan L, Anghelina M, Kantor T, Jones D, Ramadan E, Xiang Y, Huang K, Kolipaka A, Malarkey W, Ghasemzadeh N, Mohler PJ, Quyyumi A, Moldovan NI. A module of human peripheral blood mononuclear cell transcriptional network containing primitive and differentiation markers is related to specific cardiovascular health variables. *PLoS One*. 2014; 9:e95124. [PubMed: 24759906]
28. Pricop L, Salmon JE, Edberg JC, Beavis AJ. Flow cytometric quantitation of attachment and phagocytosis in phenotypically-defined subpopulations of cells using PKH26-labeled Fc gamma R-specific probes. *J Immunol Methods*. 1997; 205:55–65. [PubMed: 9236915]
29. Wilk MB, Gnanadesikan R. Probability plotting methods for the analysis of data. *Biometrika*. 1968; 55:1–17. [PubMed: 5661047]
30. Jolliffe, IT. *Principal Component Analysis*. Springer-Verlag; New York, NY: 2002.
31. Pecot, T.; Singh, S.; Caserta, E.; Huang, K.; Machiraju, R.; Leone, G. Non-parametric cell nuclei segmentation based on a tracking over depth from 3D fluorescence confocal images. 9th IEEE International Symposium On Biomedical Imaging: from nano to macro; 2012; 2013. p. 170-173.
32. Butt OI, Carruth R, Kutala VK, Kuppusamy P, Moldovan NI. Stimulation of peri-implant vascularization with bone marrow-derived progenitor cells: monitoring by in vivo EPR oximetry. *Tissue Eng*. 2007; 13:2053–2061. [PubMed: 17518714]
33. Ivanovska I, Swift J, Harada T, Pajeroski JD, Discher DE. Physical plasticity of the nucleus and its manipulation Methods. *Cell Biol*. 2010; 98:207–220.
34. Li Q, Kumar A, Makhija E, Shivashankar GV. The regulation of dynamic mechanical coupling between actin cytoskeleton and nucleus by matrix geometry. *Biomaterials*. 2014; 35:961–969. [PubMed: 24183171]
35. Moldovan L, Moldovan NI, Sohn RH, Parikh SA, Goldschmidt-Clermont PJ. Redox changes of cultured endothelial cells and actin dynamics. *Circ Res*. 2000; 86:549–557. [PubMed: 10720417]
36. Maniotis AJ, Chen CS, Ingber DE. Demonstration of mechanical connections between integrins, cytoskeletal filaments, and nucleoplasm that stabilize nuclear structure. *Proc Natl Acad Sci U S A*. 1997; 94:849–854. [PubMed: 9023345]
37. Wake K, Kawai Y, Smedsrod B. Re-evaluation of the reticulo-endothelial system. *Ital J Anat Embryol*. 2001; 106:261–269. [PubMed: 11729964]
38. Yam PT, Theriot JA. Repeated cycles of rapid actin assembly and disassembly on epithelial cell phagosomes. *Mol Biol Cell*. 2004; 15:5647–5658. [PubMed: 15456901]
39. Gampel A, Moss L, Jones MC, Brunton V, Norman JC, Mellor H. VEGF regulates the mobilization of VEGFR2/KDR from an intracellular endothelial storage compartment. *Blood*. 2006; 108:2624–2631. [PubMed: 16638931]
40. Sefton MV, Babensee JE, Woodhouse KA. Innate and adaptive immune responses in tissue engineering. *Semin Immunol*. 2008; 20:83–85. [PubMed: 18221888]
41. Chen CS, Alonso JL, Ostuni E, Whitesides GM, Ingber DE. Cell shape provides global control of focal adhesion assembly. *Biochem Biophys Res Commun*. 2003; 307:355–361. [PubMed: 12859964]
42. Green KJ, Talian JC, Goldman RD. Relationship between intermediate filaments and microfilaments in cultured fibroblasts: evidence for common foci during cell spreading. *Cell Motil Cytoskeleton*. 1986; 6:406–418. [PubMed: 3757072]

43. Laporte D, Ojkc N, Vavylonis D, Wu JQ. alpha-Actinin and fimbrin cooperate with myosin II to organize actomyosin bundles during contractile-ring assembly. *Mol Biol Cell*. 2012; 23:3094–3110. [PubMed: 22740629]
44. Ivanov AI, McCall IC, Babbin B, Samarin SN, Nusrat A, Parkos CA. Microtubules regulate disassembly of epithelial apical junctions. *BMC Cell Biol*. 2006; 7:12. [PubMed: 16509970]
45. Mavrikis M, Azou-Gros Y, Tsai FC, Alvarado J, Bertin A, Iv F, Kress A, Brasselet S, Koenderink GH, Lecuit T. Septins promote F-actin ring formation by crosslinking actin filaments into curved bundles. *Nat Cell Biol*. 2014
46. Stratman AN, Saunders WB, Sacharidou A, Koh W, Fisher KE, Zawieja DC, Davis MJ, Davis GE. Endothelial cell lumen and vascular guidance tunnel formation requires MT1-MMP-dependent proteolysis in 3-dimensional collagen matrices. *Blood*. 2009; 114:237–247. [PubMed: 19339693]
47. Anghelina M, Krishnan P, Moldovan L, Moldovan NI. Monocytes/macrophages cooperate with progenitor cells during neovascularization and tissue repair: conversion of cell columns into fibrovascular bundles. *Am J Pathol*. 2006; 168:529–541. [PubMed: 16436667]
48. Simionescu M, Simionescu N, Palade GE. Partial chemical characterization of the anionic sites in the basal lamina of fenestrated capillaries. *Microvasc Res*. 1984; 28:352–367. [PubMed: 6521660]
49. Wong AJ, Pollard TD, Herman IM. Actin filament stress fibers in vascular endothelial cells in vivo. *Science*. 1983; 219:867–869. [PubMed: 6681677]
50. Tojkander S, Gateva G, Lappalainen P. Actin stress fibers--assembly, dynamics and biological roles. *J Cell Sci*. 2012; 125:1855–1864. [PubMed: 22544950]
51. Burke TA, Christensen JR, Barone E, Suarez C, Sirotkin V, Kovar DR. Homeostatic actin cytoskeleton networks are regulated by assembly factor competition for monomers. *Curr Biol*. 2014; 24:579–585. [PubMed: 24560576]
52. Shindo A, Wallingford JB. PCP and septins compartmentalize cortical actomyosin to direct collective cell movement. *Science*. 2014; 343:649–652. [PubMed: 24503851]
53. Rasband MN. Cytoskeleton: axons earn their stripes. *Curr Biol*. 2013; 23:R197–R198. [PubMed: 23473560]
54. Kovac B, Teo JL, Makela TP, Vallenius T. Assembly of non-contractile dorsal stress fibers requires alpha-actinin-1 and Rac1 in migrating and spreading cells. *J Cell Sci*. 2013; 126:263–273. [PubMed: 23132927]
55. Heath JP. Behaviour structure of the leading lamella in moving fibroblasts I. Occurrence and centripetal movement of arc-shaped microfilament bundles beneath the dorsal cell surface. *J Cell Sci*. 1983; 60:331–354. [PubMed: 6348051]
56. Buccione R, Orth JD, McNiven MA. Foot and mouth: podosomes, invadopodia and circular dorsal ruffles. *Nat Rev Mol Cell Biol*. 2004; 5:647–657. [PubMed: 15366708]
57. Wang JH, Goldschmidt-Clermont P, Moldovan N, Yin FC. Leukotrienes and tyrosine phosphorylation mediate stretching-induced actin cytoskeletal remodeling in endothelial cells *Cell Motil Cytoskeleton*. 2000; 46:137–145.
58. Flusberg DA, Numaguchi Y, Ingber DE. Cooperative control of Akt phosphorylation, bcl-2 expression, and apoptosis by cytoskeletal microfilaments and microtubules in capillary endothelial cells. *Mol Biol Cell*. 2001; 12:3087–3094. [PubMed: 11598193]
59. Carlson AL, Florek CA, Kim JJ, Neubauer T, Moore JC, Cohen RI, Kohn J, Grumet M, Moghe PV. Microfibrous substrate geometry as a critical trigger for organization, self-renewal, and differentiation of human embryonic stem cells within synthetic 3-dimensional microenvironments. *FASEB J*. 2012; 26:3240–3251. [PubMed: 22542683]
60. Tung JJ, Tattersall IW, Kitajewski J. Tips, stalks, tubes: notch-mediated cell fate determination and mechanisms of tubulogenesis during angiogenesis. *Cold Spring Harb Perspect Med*. 2012; 2:a006601. [PubMed: 22355796]
61. Little M, Georgas K, Pennisi D, Wilkinson L. Kidney development: two tales of tubulogenesis. *Curr Top Dev Biol*. 2010; 90:193–229. [PubMed: 20691850]
62. Ghabrial AS, Levi BP, Krasnow MA. A systematic screen for tube morphogenesis and branching genes in the *Drosophila* tracheal system. *PLoS Genet*. 2011; 7:e1002087. [PubMed: 21750678]

63. Tepper OM, Capla JM, Galiano RD, Ceradini DJ, Callaghan MJ, Kleinman ME, Gurtner GC. Adult vasculogenesis occurs through in situ recruitment, proliferation, and tubulization of circulating bone marrow-derived cells. *Blood*. 2005; 105:1068–1077. [PubMed: 15388583]
64. Moldovan NI, Goldschmidt-Clermont PJ, Parker-Thornburg J, Shapiro SD, Kolattukudy PE. Contribution of monocytes/macrophages to compensatory neovascularization: the drilling of metalloelastase-positive tunnels in ischemic myocardium. *Circ Res*. 2000; 87:378–384. [PubMed: 10969035]
65. Hamilton NB, Attwell D, Hall CN. Pericyte-mediated regulation of capillary diameter: a component of neurovascular coupling in health and disease. *Front Neuroenergetics*. 2010; 2
66. Moldovan L, Irani K, Moldovan NI, Finkel T, Goldschmidt-Clermont PJ. The actin cytoskeleton reorganization induced by Rac1 requires the production of superoxide. *Antioxid Redox Signal*. 1999; 1:29–43. [PubMed: 11225730]
67. Tousoulis D, Kampoli AM, Stefanadis C. Diabetes mellitus and vascular endothelial dysfunction: current perspectives. *Curr Vasc Pharmacol*. 2012; 10:19–32. [PubMed: 22112354]
68. Eleftheriadis T, Antoniadi G, Pissas G, Liakopoulos V, Stefanidis I. The renal endothelium in diabetic nephropathy. *Ren Fail*. 2013; 35:592–599. [PubMed: 23472883]

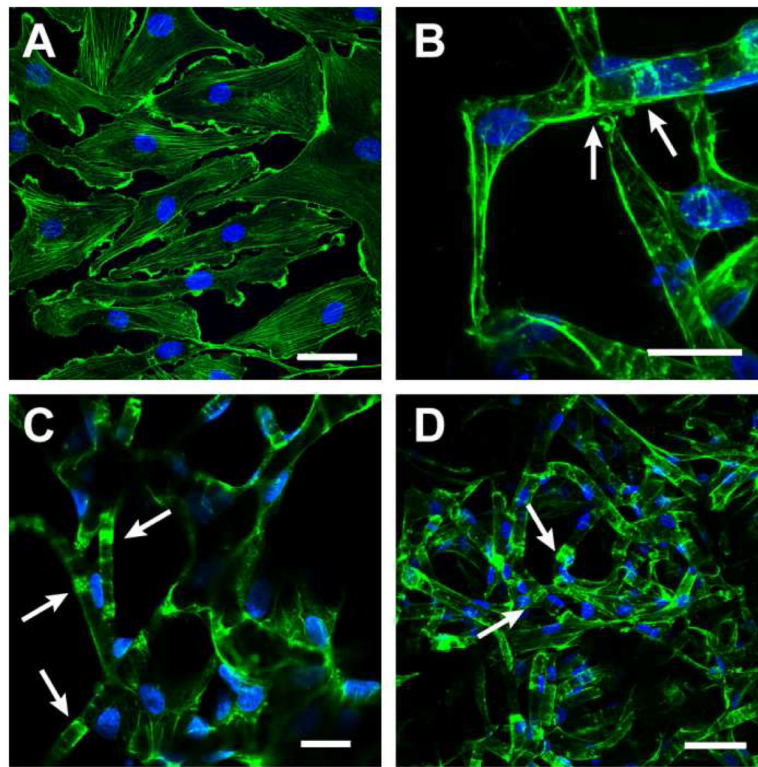


Figure 1. Distribution of F-actin in cells interacting with PCL supports

A. HUVECs cultured for 1 day in endothelial growth medium on a TCPS coverslip, showing F-actin organized as classical stress fibers and marginal ruffles. **B.** When seeded on micro-fibrillar PCL scaffolds for 1 day, same HUVECs organized their F-actin with respect to SMFs in both parallel, but also transversal bundles (arrows). **C.** In long-term (10 days) cultures of HUVECs on PCL fibers, most of the F-actin was organized in transversally banded structures (arrows). **D.** Transversal bands were present, but scarcer in the more primitive ECFCs at 10 days of cultivation (arrows). In all images, F-actin was detected by phalloidin-AF488 (green) and nuclei by DAPI (blue). Scale bars: A, D: 50 μm ; B, C: 20 μm .

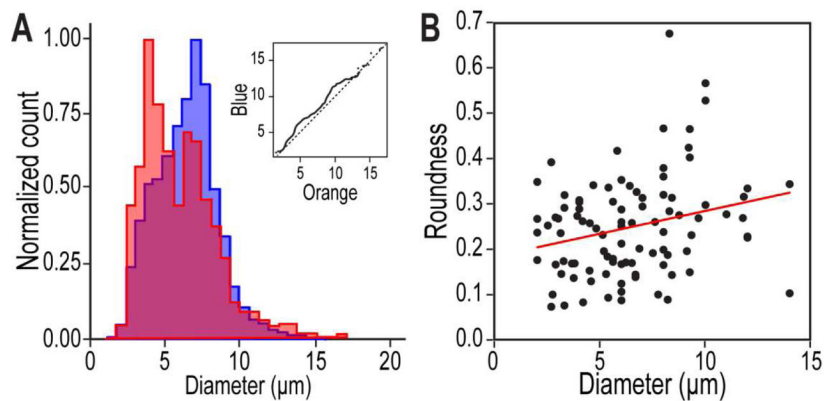


Figure 2. Relationship between SMFs diameter at HUVECs attachment sites and nuclear shape
A. Distribution of fiber diameters at the cell attachment points (orange) as compared to overall SMFs diameters (blue), indicates the preference of cells localization on thinner fibers. *Inset:* Dissimilarity of the two distributions, verified by quantile Q-Q plotting. **B.** Relationship of nuclear roundness (defined in the Methods section) with fiber diameter at the cell-attachment site ($R^2= 0.06$, $p=0.01$; number of analyzed cells, $n= 95$).

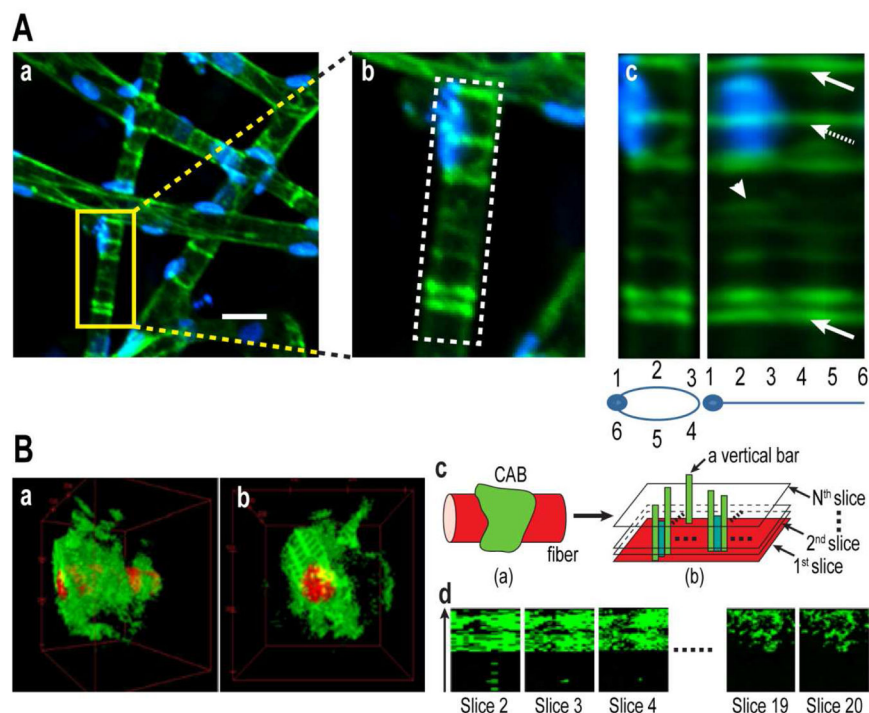


Fig. 3. Demonstration of full-circle wrapping of SMFs by F-actin in HUVECs

A. F-actin in HUVECs cultured on SMFs for 10 days. **a**, 2D projection of the original confocal image stack; **b**, enlarged SFM portion containing F-actin bands of interest; **c**, vertically-aligned 2D image projection (left), compared with its digital unwrapping (right), showing full-circle continuity of F-actin around the SMF (arrows), one of them overlapping with the nucleus (hashed arrow); other bands represent shorter ‘concave actin bundles’ (CAB; e.g. arrowhead; compare with Fig. 4). **B.** F-actin distribution in HUVECs after short-term incubation (1 day): side (**a**) and front (**b**) views of reconstituted 3D image (note the stripped pattern of F-actin in the fiber-transverse structures); **c**, sketch showing the procedure to obtain the pixel intensities in cylindrical planes around the SMF; **d**, serial displays of pixel distribution in successive cylindrical planes placed at increasing distances from SMF (note the continuity of actin at shorter distances from the fiber); the arrow indicates SMF cylinder’s axis.

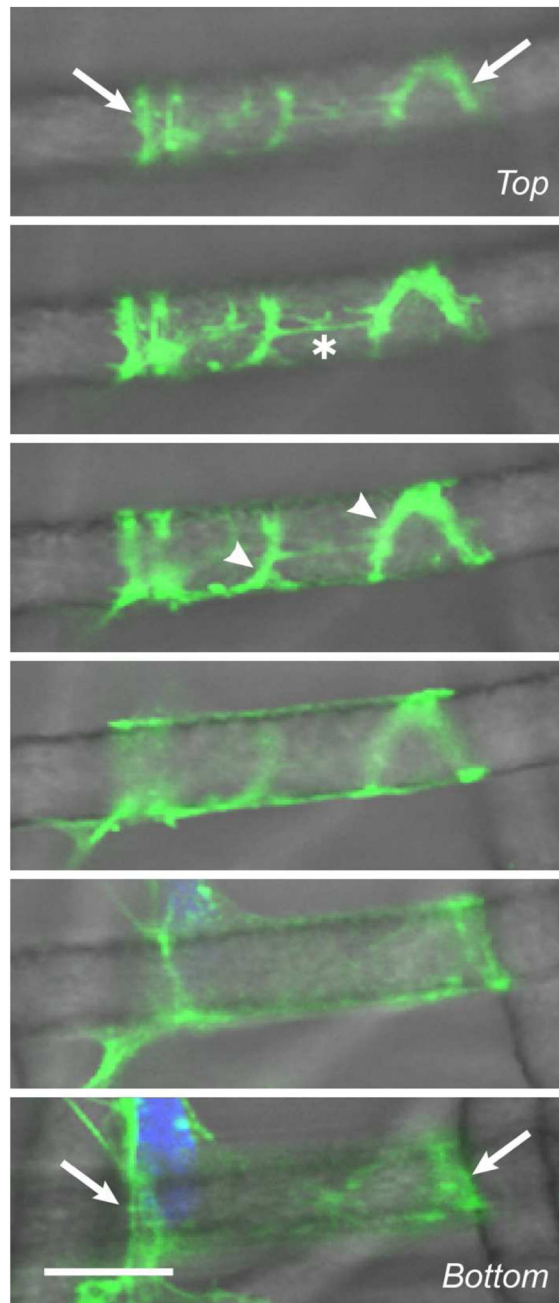


Figure 4. Model of AGs formation by reorientation of shorter F-actin bundles

Confocal optical sectioning of a whole cell from the top to bottom (including nucleus) side of a fiber. Note that both fully circumferential, transversally oriented AGs (arrow), but also shorter and oblique segments (arrowheads) are present in the same cell, as possible stages of a sequential AGs formation process. Remnants of horizontal stress fibers are also visible (asterisk). Phalloidin (green) and DAPI (blue) staining. Scale bar, 10 μm .

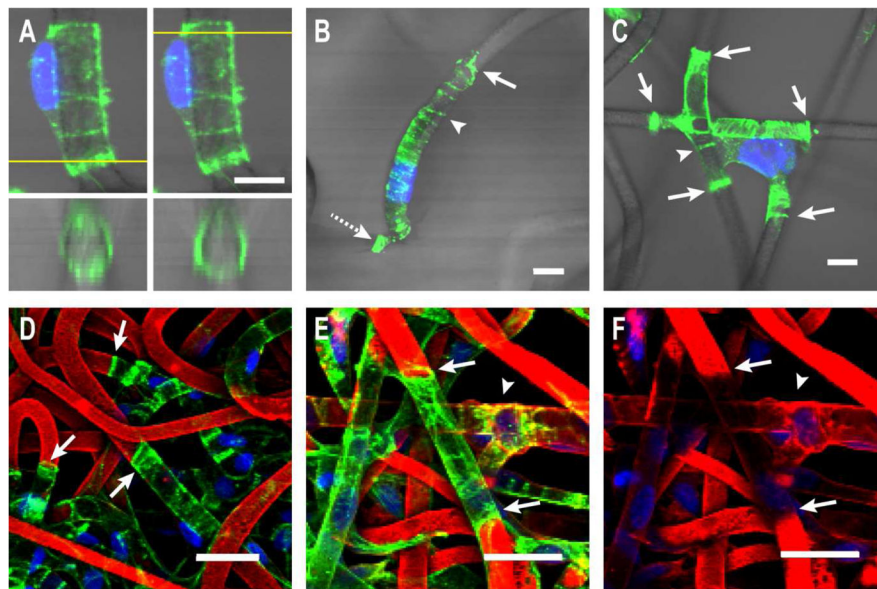


Figure 5. Structure and function of F-actin rings during cell-scaffold interaction

A. Optical sections through a SMF-attached cell show that AGs (F-actin bands) completely surround the fiber at the cell's extremities (yellow line). **B.** Imaging of F-actin in a SMF-attached cell shows many AGs (arrowhead), but also a peripheral undulated actin ruffle-like structure (arrow), and an actin-rich blob (reminiscent of an uropod, dashed arrow). **C.** One single cell spreading over three intersecting SMFs presents marginal AGs at all extremities (arrows), usually thicker than those at the cell's interior (arrowhead). **D.** Sharp color transitions (arrows) on SMFs stained with PKH26 (red) after cell wrapping, indicate a tight apposition between cells and SMFs, that prevents the stain to diffuse under cells. **E, F.** A cell limited by an AG (**E**, arrows; overlay of red and green channels), blocking lateral diffusion of the stain underneath the cell (**F**, arrows, red channel only for comparison). This was found in regions occupied by cells, but not where the AGs were missing (arrowhead). F-actin was stained with phalloidin-AF488 (green), nuclei with DAPI (blue). SMFs in **A–C** were visualized by DIC microscopy. Fibers in **D–E** were stained with PKH26 (red). In all cases, the images are two dimensional projections of confocal z-stacks. Scale bars: **A–C**: 10 μm; **D–F**: 30 μm.

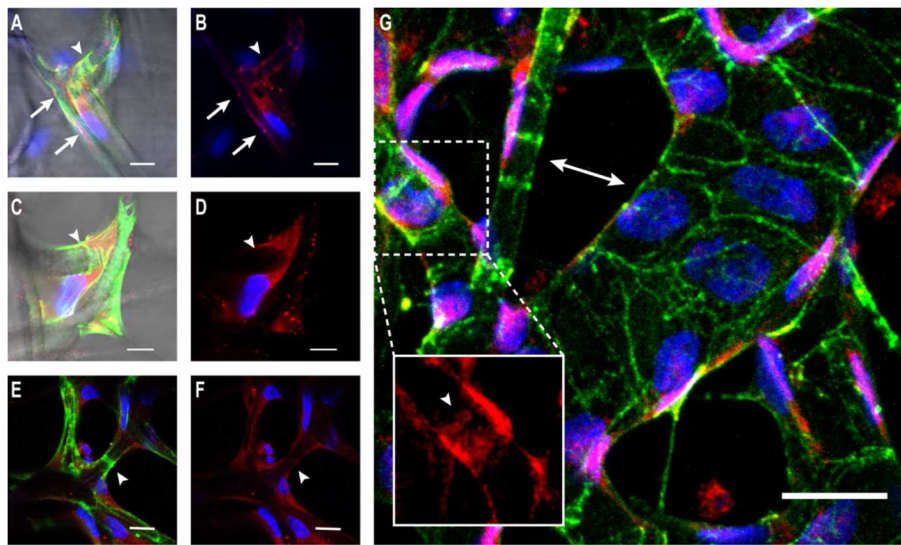


Figure 6. Assessment of molecular composition of AGs

A, B. Immuno-detection of vinculin (red) at the ends of F-actin containing stress fibers longitudinally aligned with the SMF (arrows), but not in an adjacent AG (green, arrowheads). **C, D.** Absence of the FA protein paxillin (arrowhead, right image) in an F-actin stained AG (arrowhead, left image). **E, F.** Lack of association of AG (arrowhead) with the vimentin-positive intermediate filaments. **A–F:** on left there are overlays of red (antibody) and green (F-actin) channels, and on right the respective red-only channel for comparison. As commonly encountered in cultured cells, FA components are also abundantly present in a peri-nuclear compartment within cytoplasm. **G.** Detection of alpha-actinin in AGs (insert, arrowhead). Compare the organization of F-actin in transversal AGs within cells that fully wrap small-caliber fibers, but not in cells attached to scaffolds of larger diameter (double-headed arrow). In **A–G**, F-actin was stained with phalloidin-AF488 (green), the antigens detected with secondary antibodies conjugated with AlexaFluor-647 (red), and the nuclei with DAPI (blue). Fibers in **A** and **C** were visualized by DIC microscopy. All images are two-dimensional projections of confocal z-stacks. Scale bars: **A–F**; 10 μm ; **G**: 20 μm .

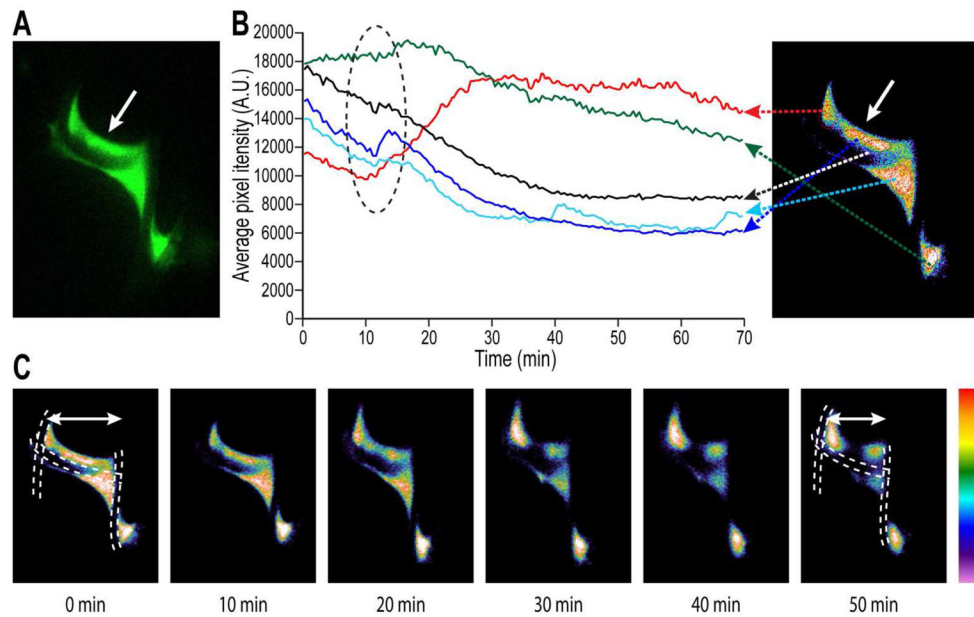


Figure 7. Dynamics of F-actin within scaffold-attached cells

A. Initial positioning of a GFP-actin labelled cell at the intersection of three SMFs (dashed lines in **C**; compare to Fig. 4C). Optical sectioning through an AG is shown (arrow). **B.** Time-dependent pixel intensities in different regions of the image (distinguished by lines color). Note the coincident variation in fluorescence within the same AG seen from opposite positions to the main SMF (deep blue track originates from the portion of the cell above the fiber, and the light blue track from below it), and independently of the regions at cell's extremities (red and green tracks). Also remarkable are the abrupt but simultaneous changes in intensity in different portions of the cell, indicative of a coordinated cytoskeletal remodeling event (dashed circle on the graph). Increase in the intensity of the upper-corner region (red line), argues that the changes were not the result of GFP label's photo-bleaching. **C.** Snapshots at 10-min intervals illustrating the deformation of the cell-fiber system; coincident with changes in F-actin distribution, note the displacements of the extremities of the cell attached to the crossing SMFs (double-headed arrows). Vertical bar indicates the color-coded pixel intensity (in arbitrary units).

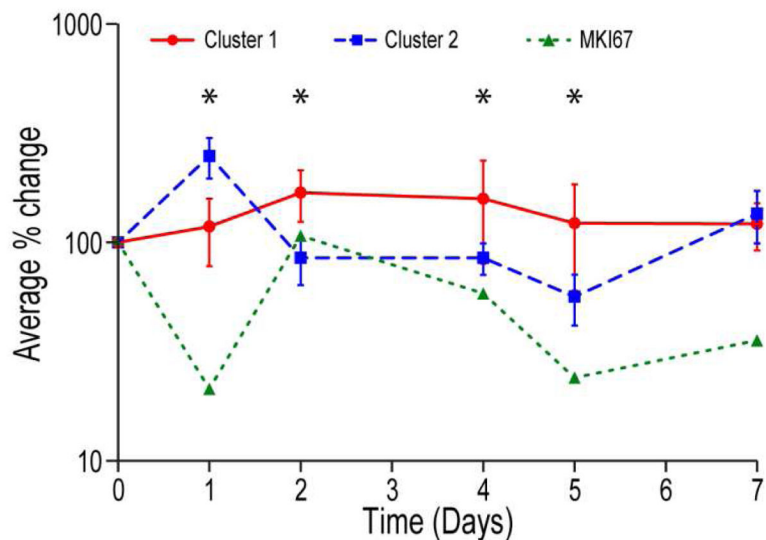


Figure 8. Time course of the expression of endothelial differentiation markers in SMFs-attached HUVECs

Averaged changes (vs. time=0) of relative copy numbers (RCNs) of endothelial/vascular function-related markers CD117, CD31, CD34, CDH5, KDR, NES, NOS3, TEK, VWF and of ACTA2 (Cluster 1, n=10), of several primitive and/or endothelial function-indifferent genes ABCG2, ALPL, CAV3, CD133, CNN1, COL1A1, FSHR, GATA4, NKX2-5, POUF5F1 (Cluster 2, n=10), and of the proliferation marker gene MKI67. As reference (time=0), we used the corresponding RCN values of genes as expressed in the same cells collected from TCPS dishes, just before the transfer on SMFs. Of note, the very poor growth of HUVECs on PCL films ([20–24] and our observations) prevented us from using this condition as reference. Note that at 1day post-seeding the cells in scaffolds presented the highest values of non-relevant genes (lowest differentiation, combined with a ‘dormant’ state reflected in lowest value of MKI67 expression, as compared to the slightly subconfluent HUVEC cultures on TCPS), that decreased and remained so thereafter for a week. Data represent on a log scale the percent change of RCN vs. time=0, averaged for all 10 genes in each cluster \pm SD (* p <0.001 for time point-specific inter-cluster comparison).